NMR Setup for Polarization Measurements of Polarized ^3He Target

Makhsud Rasulbaev

Department of Physics, Major in Nuclear Physics
The Graduate School

Supervised by Professor Wooyoung Kim

Approved as a qualified thesis of Makhsud Rasulbaev
for the degree of Master of Science
by the Evaluation Commitee

December 2003

Chairman _____

_____

_____

The Graduate School Council, Kyungpook National University

Abstract

The main goal of this research is to make the first step to design and construct the NMR setup for the polarization measurements of the polarized ^3He target. Experimental setup including the Helmholtz coils and NMR electronics has been constructed, tested and calibrated using a free radical 2,2-Diphenyl-1-Pycrilhydrasil. The setting is optimized for the purpose of Adiabatic Fast Passage technique of NMR. Electronics and software instability modes are found and efforts are made to avoid the instability. Procedures for reaching high signal to noise ratio are investigated. This thesis focuses on the experimental setup and contains the description of polarization processes and theory of the polarization measurements. The results for the setup, test and calibration are presented in this thesis.

Contents

List of Figures

List of Tables

Chapter 1

Introduction

The theory of quantum chromodynamics is used to explain the substructure of the neutron [1, 2]. Scattering experiments with polarized electron beams and polarized target test this theory by studying the quark structure of the neutron. Ideally, the polarized neutron targets would be used in scattering experiments, but a free neutron has a half-life of 10.23 minutes [3]. A stable alternative to a free neutron is a ^3He nucleus.

In the ^3He ground state, the nucleus is predominantly in the S-state from which the spins of the two protons are anti-aligned. This configuration effectively cancels the proton spin contribution to the nuclear magnetic moment [4]. Thus, with slight corrections for the residual photon effect [5], the ^3He nuclear spin is dominated by that of the neutron. Scattering experiments [6-10] that study neutron structure therefore often use polarized ^3He targets.

Polarized ^3He produced by spin exchange with optically pumped Rb metal is used for precision measurements of the neutron spin structure functions, tests of fundamental symmetries [11], neutron polarizers and and for MRI of the human body [12, 13]. In many of these cases it is important to know accurately the ab-

solute ^3He polarization. At present, the most common method of polarimetry is Nuclear Magnetic Resonance (NMR) usually on the base technique of adibatic fast passage(AFP) [14]. While the signal-to-noise ratio provided by this technique is excellent, absolute measurements require a complicated calibration which usually has a limited precision [15, 16].

Our main goal was to construct the NMR Setup for ^3He polarization and polarimetry measurements facilities. System described in this thesis is a first step towards creating it. Experimental setup has been constructed, calibrated and tested on DPPH sample.

This thesis is organized as follows. Chapter 2 starts with the definition of rate of polarization and describes most common techniques of polarization for ^3He target. Factors affecting polarization are listed. Chapter 3 focuses on Adiabatic Fast Passage technique of Nuclear Magnetic Resonance. The behavior of a magnetic moment (^3He nucleus) in a magnetic field is discussed. It is shown that a magnetic moment precesses about the magnetic field at a specific frequency (the Larmor frequency). The effect of adding a rotating field is then detailed, and the resonance condition is found. Bloch equations, the conditions for the adiabatic fast passage and the effect of passing through resonance are delivered. Chapter 4 describes experimental setup, its calibration, experimental procedures and performance of the equipment during the run. Instrument synchronization is also noted. Finally Chapter 5 presents the results and discussion of our experiment.

Chapter 2

Polarization Processes

This chapter starts with the definition of rate of polarization, describes most common techniques of polarization for ^3He target. Factors affecting polarization are listed.

2.1 Optical Pumping and Spin Exchange

There are two techniques commonly used for polarizing ^3He. One technique uses direct optical pumping of the metastable 2 $^3S_1$ state of ^3He. While high nuclear polarization can be obtained the use of this technique for high density target is difficult because the ^3He density has to be low to maintain RF discharge. Second technique, in which ^3He is polarized by a two steps process. First, Rb vapor is polarized by optical pumping with circularly polarized light. Second, the Rb electron polarization is transferred to the ^3He nucleus by spin exchange interaction.

The process that provides the ^3He nucleus with its polarization is that of a spin-exchange with electron-spin polarized alkali-metal atoms. Alkali metals are used because these gases have only one outer shell electron, thus effectively providing a spin of 1/2. Rubidium is polarized to near 100% by means of optical pumping using

lasers with a wavelength of 795 nm. A hyperfine interaction between the Rubidium atom and the ^3He nucleus then transfers the spin from the Rb to the ^3He during binary collisions, thus polarizing the ^3He.

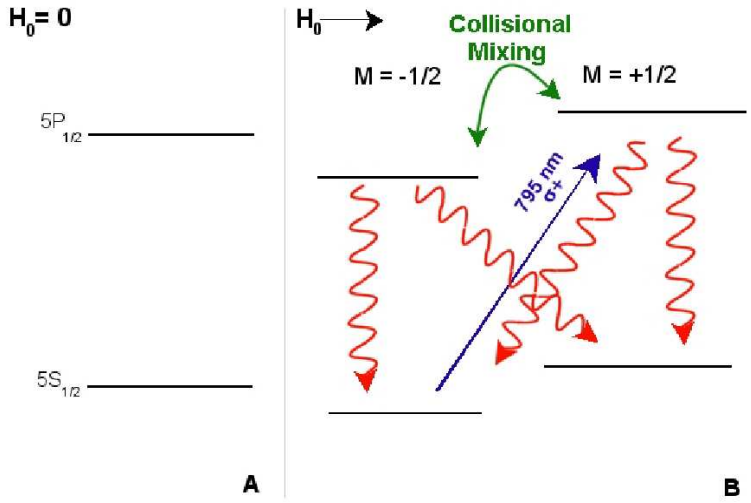

Fig 2.1: The *Rb* energy states without a magnetic field (A) and the Zeeman splitting of the *Rb* energy states due to a magnetic field H_0 (B) from the main coils.

The principle of optical pumping is illustrated in the Figure 2.1. In this figure the nuclear spin of the Rb is not shown and the relevant atomic states are the $S_{1/2}$ and $P_{1/2}$ states, each with two magnetic substates $M = \pm 1/2$. Additional hyperfine splitting is introduced by the *Rb* nuclear spin. However broad-bandwidth laser light can be used to optically pump from all of the hyperfine levels of *Rb*. Circularly polarized light with spin projection $+1(\sigma)$ can only be absorbed by the $S_{1/2}$ with $M = -1/2$. This populates the $P_{1/2}$ sublevel with $M = +1/2$, which can decay radiatively to either sublevel of the ground state. The relative radiative decay rates are given by the Clebsch-Gordon coefficients, 2/3 and 1/3, corresponding to the $M = -1/2$ and the $M = +1/2$, ground states respecively. However, if

allowed to decay radiatively, the photon emitted can have any polarization and can be reabsorbed by the other Rb atoms, resulting in the depolarization of the gas. This is more likely to occur when the gas is dense, as is the case within the glass cells. Small amounts of N_2 gas are used as a buffer so that when the excited Rb atom collides with the N_2, the Rb will decay back to the ground state by giving the N_2 its energy rather than emitting a photon. Approximately 60 torr of N_2 is used in combination with 7600 torr (at room temperature) of ^3He. This pressure specification has previously been shown experimentally to be the proper amount of N_2 for high collision rates without affecting the ^3He nuclei being studied [17, 18]. In addition, collisions with the ^3He and N_2 gases will randomize the P states and the relative decay probabilities to each sublevel of the ground state become 50%.

The ^3He nucleus is polarized by the spin-exchange with automatically polarized Rb. A hyperfine interaction occurs between the Rb atomic spin and the ^3He nuclear spin during collisions. Polarization is transferred from the outer shell Rb electron to the ^3He nucleus, and the Rb is then quickly repolarized by the laser light. The rate of ^3He polarization by the Rb is given by the following differential equation,

$$\frac{dP_{He}(t)}{dt} = \gamma_{SE}(\langle P_{Rb}\rangle - \langle P_{He}(t)) - \Gamma P_{He}(t) \tag{2.1}$$

where a $< P_{Rb} >$ is the average Rb polarization (approximately 100%), P_{He} is the ^3He polarization, γ_{SE} is the spin exchange rate between the Rb and ^3He, and Γ is the overall depolarization rate of the ^3He due to all possible depolarization mechanisms. The spin exchange rate is given by the following expression:

$$\gamma \propto [Rb][^3He]\sigma_{SE}, \tag{2.2}$$

where $[Rb]$ and $[^3He]$ are the concentrations of each gas and σ_{SE} is the probability of a spin-exchange occurring. Therefore, an increased amount of each gas will provide more collisions. However, control can only be exerted over the density of the Rb gas,

as the amount of ^3He is fixed. To do so, the temperature of the Rb is increased or decreased by varying the temperature of the oven surrounding the pumping chamber. This causes an increase or a decrease in the density of the Rb vapor. If the density is increased, a larger spin exchange rate will result, which will yield a larger P_{He}. Additional laser power is also required to polarize the larger amount of Rb. On the other hand, if the density is decreased, a lower spin exchange rate is produced, and a lower P_{He} is the outcome.

Solving equation (2.1), the ^3He polarization is expressed as follows,

$$P_{He}(t) = \frac{\gamma_{SE}}{\gamma_{SE} + \Gamma}\langle P_{Rb}\rangle(1 - e^{-(\gamma_{SE}+\Gamma)t}) \tag{2.3}$$

where at $t = \infty$, $P_{He}^{max} = \frac{\gamma_{SE}}{\gamma_{SE}+\Gamma}\langle P_{Rb}\rangle$. So if $\gamma_{SE} \gg \Gamma$, $P_{He}^{max} \approx \langle P_{Rb}\rangle \approx 100\%$ [24].

Therefore to achieve maximum polarization and the maximum polarization rate, it is necessary to make Γ as small as possible, or equivalently, the relaxation time, $T = 1/\Gamma$, large. Although 100% polarization can theoretically be achieved, experimentally, the largest polarization achieved for these targets is around 50%, with a typical value of about 35%.

2.2 Factors Affecting Polarization

The spin exchange rate γ_{SE} is described by

$$\gamma_{SE} \propto k_{SE}[Rb] \tag{2.4}$$

If it is assumed that the probability of spin-exchange k_{SE} is constant, γ_{SE} can only increase only by raising the Rb vapor concentration $[Rb]$ in the cell. At very high densities, however, the Rb vapor becomes optically opaque which prevents uniform absorption of the circularly polarized light needed for Rb optical pumping. With

the present setup, it has been found experimentally by Thomas Jefferson National Accelerator Facility (TJNAF) ^3He group that the optimum Rb density occurs at about $170°C$.

The depolarization rate Γ can be expressed as the inverse of a relaxation time $T = 1/\Gamma$. The following factors contribute to shortening T:

1. ^3He collisions with cell wall paramagnetic impurities. Microfissures in the cell walls increase the number of collisions by increasing surface area and trapping ^3He atoms. (typical TJNAF target cell $T \approx 80$ hours)

2. Magnetic dipole-dipole interactions between ^3He nuclei [25] (calculated theoretically for the targets used at TJNAF, $T \approx 84$ hours).

3. Magnetic holding field gradients [26, 27] (coils of $1.0m$ diameter give $T \approx 1000hours$)

   An inhomogeneous magnetic field (to produce the magnetic holding field in the target system, large Helmholtz coils are used to ensure a small field gradient which results in a value of $T \approx 1000$ hours)

4. Wall collisions with impurities within the target cell. Gas impurities and wall collisions are the largest contributing factors, and can in principle be controlled in the laboratory. These last two contributions determine the polarization rate, and the maximum polarization in manufactured cells. Collisions occur between ^3He and impurities in both the cell and the gas. Microfissures in the glass contribute to the depolarization of the ^3He by trapping ^3He molecules, thus increasing the chances that the gas collides with the walls of the cell. Cell wall collisions, is inherently related to cell construction and design. Potential improvements include using a cell wall coating [28], a new cell shape, other

types of glasses, a different cell filling procedure, or an entirely new cell wall material.

Chapter 3

Theory of Polarization Measurement

Nuclear Magnetic Resonance (NMR) is used to measure the ^3He polarization using a technique called adiabatic fast passage (AFP)[14]. This process involves manipulating the ^3He nuclear spin using time-dependent magnetic fields. First, the energy of a magnetic moment (^3He nucleus) in a magnetic field will be discussed. It will be shown that a magnetic moment precesses about the magnetic field at a specific frequency (the Larmor frequency). The effect of adding a rotating field will then be detailed, and the resonance condition will be found. Next, it will be explained how a rotating magnetic field is obtained in practice. Finally, the conditions for the adiabatic fast passage and the effect of passing through resonance will be delivered.

3.1 Behavior of a Magnetic Moment in a Magnetic Field

A. Energy of a Magnetic Moment in a Magnetic Field

The magnetic moment of a nucleus is defined as

$$\vec{\mu} = \gamma \hbar \vec{J} \tag{3.1}$$

Here, γ is the gyromagnetic ratio (a constant particular for each nucleus with the units $\frac{1}{s \bullet G}$ and $\hbar\vec{J}$ is the total angular momentum (the vector sum of the spin and orbital angular momenta of the nucleus). It is well known that the energy E of a magnetic moment μ in a magnetic field $\vec{H}$ is

$$E = -\vec{\mu} \cdot \vec{H} \tag{3.2}$$

By choosing the quantization axis $\hat{z}$ aligned with the magnetic field $\vec{H} = H\vec{z}$, Eq. (3.1) and Eq. (3.2) are combined to establish the nuclear spin energy eigenstates

$$E = -\gamma \hbar \vec{H} \cdot \vec{J} = -\gamma \hbar H J_z \tag{3.3}$$

where J_z is the component of total angular momentum along $\hat{z}$ and has eigenvalues $(-J, -J+1, ..., J-1, J)$. The energy difference between neighboring ($\Delta J_z = \pm 1$) eigenstates is

$$\Delta E = \gamma \hbar H \tag{3.4}$$

This energy corresponds to that of the photon that is emitted or absorbed during a transition between the two states. For a nucleus with gyromagnetic ratio γ in a magnetic field H , the photon frequency necessary for transitions between energy levels is

$$\omega = \gamma H. \tag{3.5}$$

B. Precession in a magnetic field

A nucleus of magnetic moment μ in a magnetic field $\vec{H}$ experiences a torque

$$\vec{N} = \vec{\mu} \times \vec{H} \tag{3.6}$$

A torque produces a change in angular momentum. Eq. (3.6) therefore can be rewritten as

$$\frac{d(\hbar\vec{J})}{dt} = \vec{\mu} \times \vec{H} \tag{3.7}$$

By substituting for $\hbar\vec{J}$ using Eq. (3.1), Eq. (3.7) becomes

$$\frac{d(\vec{\mu})}{dt} = \gamma(\vec{\mu} \times \vec{H}) \tag{3.8}$$

The transformation of the time derivative $\frac{d\vec{V}(t)}{dt}$ of any time-dependent vector $\vec{V}(t)$ to its time derivative $\frac{\delta\vec{V}(t)}{\delta t}$ in a frame rotating at an angular frequency $\vec{\omega'}$ is given by

$$\frac{d\vec{V}(t)}{dt} = \frac{\delta\vec{V}(t)}{\delta t} + \vec{\omega'} \times \vec{V}(t) \tag{3.9}$$

Transforming Eq. (3.8) to a frame S' rotating at the angular frequency ω' gives

$$\frac{\delta\vec{\mu}}{\delta t} + \vec{\omega'} \times \vec{\mu} = \gamma(\vec{\mu} \times \vec{\vec{H}}) \tag{3.10}$$

Simplifying Eq. (3.10) gives

$$\frac{\delta(\vec{\mu})}{\delta t} = \gamma(\vec{\mu} \times (H + \frac{\vec{\omega'}}{\gamma})) \tag{3.11}$$

The direction of the frame rotation is chosen to be counter-clockwise when viewed in the direction of the magnetic field (the $+\hat{H}$ direction). In other words, $\vec{\omega'} = \omega'(-\hat{H})$. Eq. (3.11) can now be rewritten as

$$\frac{\delta(\vec{\mu})}{\delta t} = \gamma(\vec{\mu} \times (H - \frac{\omega'}{\gamma}\hat{H})) \tag{3.12}$$

If the frame rotates at an angular frequency $\omega' = \gamma H$, the torque experienced by the magnetic moment will be

$$\frac{\delta\vec{\mu}}{\delta t} = \gamma(\vec{\mu} \times 0) = 0 \tag{3.13}$$

Eq. (3.13) shows that the magnitude and direction of $\vec{\mu}$ in this frame is constant. In the laboratory frame, this is interpreted as a precession of $\vec{\mu}$ about $\hat{H}$ with frequency ω'. The angular frequency of precession ω' about a field H is known as the Larmor frequency. It is interesting to note that this frequency $\omega' = \gamma H$ is identical to the photon frequency (Eq. (3.5)) needed to stimulate energy-level transitions.

C. The case of static and rotating fields

Now the case of a magnetic moment in a magnetic field with a rotating component $H_1[cos(\omega_1 t)\hat{x} - sin(\omega_1 t)\hat{y}]$ and a static component $H_\circ\hat{z}$ will be considered as shown in the Figure 3.1. To move to a reference frame rotating at $\vec{\omega}_1' = -\omega_1\hat{z}$, the transformations

$$\begin{aligned} \hat{z'} &= \hat{z'} \\ \hat{x'} &= cos(\omega_1 t)\hat{x} - sin(\omega_1 t)\hat{y} \\ \hat{y'} &= cos(\omega_1 t)\hat{x} + sin(\omega_1 t)\hat{x} \end{aligned} \tag{3.14}$$

are made. In this rotating frame, the combined magnetic field is $\vec{H}' = H_\circ\hat{z}' + H_1\hat{x}'$, and the change in magnetic moment (using Eq. 3.11) is

$$\frac{\delta(\mu)}{\delta t} = \gamma(\vec{\mu} \times [H_\circ\hat{z'} + H_1\hat{x'} + \frac{\vec{\omega}_1}{\gamma}]) \tag{3.15}$$

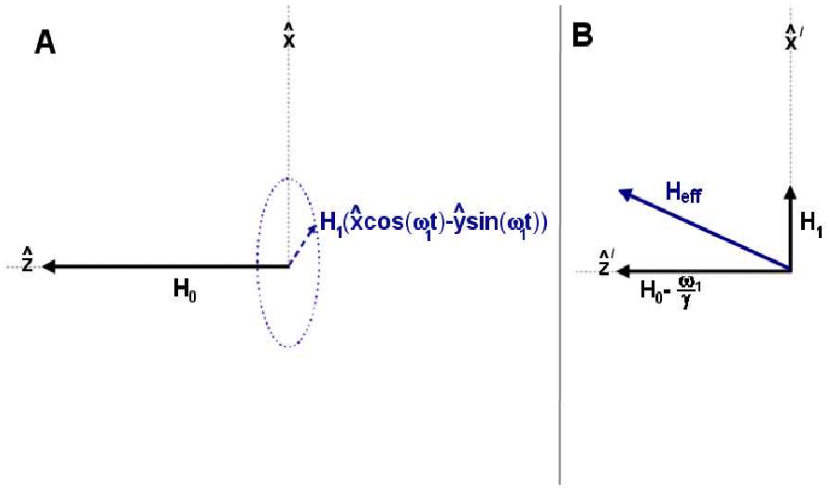

Fig 3.1: The magnetic fields in the laboratory frame (A) and the rotating frame(B).

Grouping terms gives

$$\frac{\delta(\mu)}{\delta t} = \gamma(\vec{\mu} \times [(H_\circ - \frac{\vec{\omega}_1}{\gamma})\hat{z'} + H_1\hat{x'}]) \tag{3.16}$$

An effective magnetic field (Figure 3.1)

$$\vec{H}_{eff} \equiv (H_\circ - \frac{\omega_1}{\gamma})\hat{z'} + H_1\hat{x'} \tag{3.17}$$

can now be used to simplify Eq. (3.16) to

$$\frac{\delta(\vec{\mu})}{\delta t} = \gamma(\vec{\mu} \times \vec{H}_{eff}) \tag{3.18}$$

Eq. (3.18) is the rotating frame equivalent of Eq. (3.8) with $\vec{H} = \vec{H}_{eff}$. Following the conclusion of subsection B of section 3.1, the magnetic moment will precess about $\vec{H}_{eff}$ in the rotating frame at the frequency $\omega'' = \gamma H_{eff}$.

When $|H_1| \ll |H_\circ|$, $\vec{H}_{eff}$ is nearly aligned with $\pm\hat{z'}$ unless the condition

$$|H_1| \approx |H_\circ - \frac{\omega_1}{\gamma}| \tag{3.19}$$

is satisfied. In other words, the effect of a field along $\hat{x}'$ is negligible when its angular frequency ω_1 is far from $\gamma H_\circ$. Resonance occurs when

$$\omega_1 = \gamma H_\circ \tag{3.20}$$

during which the effective magnetic field becomes

$$\vec{H}_{eff} = H_1 \hat{x}' \tag{3.21}$$

At resonance, therefore, the magnetic moment precesses about $\hat{x}'$.

D. The case of static and oscillating fields

During adiabatic fast passage (AFP), the RF coils produce a weak, oscillating magnetic field $\vec{H}_{RF} = 2H_1 cos(\omega_1 t)\hat{x}$, and the main coils produce a strong, magnetic holding field $\vec{H}_\circ = H_\circ \hat{z}$ as shown in the Figure 3.2. The oscillating field can be broken up into two counterrotating components

$$\vec{H}_{RF} = H_1[cos(\omega_1 t)\hat{x} - sin(\omega_1 t)\hat{y}] + H_1[cos(\omega_1 t) + sin(\omega_1 t)\hat{y}] \tag{3.22}$$

The first component rotates at $-\omega_1 \hat{z}$, and the second component rotates at $\omega_1 \hat{z}$. Since these fields are much weaker than the holding field $|H_1| \ll |H_\circ|$, only at resonance can they significantly affect the motion of the magnetic moment.

When the reference frame is chosen to rotate at the frequency $\vec{\omega}_1 = -\omega \hat{z}$ of the first component, resonance (Eq. (3.20)) occurs at $\omega_1 H_1$. In this frame, the first component is static along $\hat{x}'$. The second component, however, is rotating off-resonance at frequency $+2\omega_1 \hat{z}'$. Since off resonance rotating magnetic fields do not

significantly affect a magnetic moment, the second component of the oscillating field can be ignored in this reference frame.

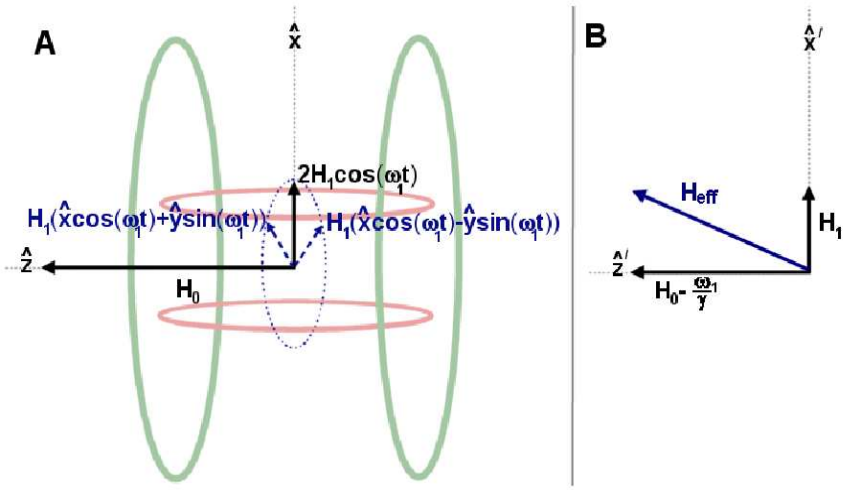

Fig 3.2: The magnetic fields used in AFP in the coordinate systems of the laboratory frame (A) and the rotating frame(B).

Neglecting the second component, the effective magnetic field in the frame rotating at $\vec{\omega}_1 = -\omega_1\hat{z}$ (Fig. 3.2) now becomes

$$\vec{H}_{eff} = (H_\circ - \frac{\omega_1}{\gamma})\hat{z}' + H_1\hat{x}' \tag{3.23}$$

Notice Eq. (3.23) is identical to Eq. (3.17). The combination of static and oscillating magnetic fields has therefore been reduced to the case described in subsection C of section 3.1. The magnetic moment will precess about $\vec{H}_{eff}$ where at resonance, $\vec{H}_{eff} = H_1\hat{x}'$.

3.2 Bloch Equations

In 1946 Felix Bloch proposed for the description of magnetic properties of ensembles of nuclei in external magnetic fields a set of very simple equations derived from the phenominological arguments, that had proved exceedingly fruitful, and for liquid gases samples at least, have provided in most cases the a correct quantitative description of the detailed behaviour of the phenomena. The heuristic argument for obtaining these equations is as follows.

First, in an arbitrary homogeneous field the equation of motion of the nuclear magnetization for an ensemble of free spins was shown to be

$$\frac{d\vec{M}}{dt} = \gamma \vec{M} \times \vec{H}. \tag{3.24}$$

Second, in a static field $H_z = H_\circ$, the trend of magnetization towards its equilibrium value $M_z = M_\circ = \chi_\circ H_\circ$ can often be described with good accuracy by the equation $\frac{dM_z}{dt} = -\frac{(M_z - M_\circ)}{T_1}$. T_1 is called the longitudinal relaxation time.

Third, if by any means such as an RF pulse, the nuclear magnetization is given a component at right angles to the applied field $H_\circ$, the various local fields, owing to the fact that the spins are actually not free but interact with each other and with their surroundings, cause the transverse magntization to decay at a rate which can often be represented by two Bloch equations

$$\frac{dM_x}{dt} = -\frac{M_x}{T_2}, \tag{3.25}$$

$$\frac{dM_y}{dt} = -\frac{M_y}{T_2} \tag{3.26}$$

where T_2 is called the transverse relaxation time.

Fourth, and this is a new assumption rather than a consequence of the three previous points, in the presence of applied field, the sum of DC field and a much

smaller RF field, the motion due to the relaxation can be superposed on the motion of the free spins, leading to the another Bloch equation

$$\frac{d\vec{M}}{dt} = \gamma\vec{M} \times \vec{H} - \frac{M_x\hat{x}' + M_y\hat{y}'}{T_2} - \frac{M_z - M_0}{T_1}\hat{z}', \tag{3.27}$$

where $\hat{x}'$, $\hat{y}'$, $\hat{z}'$ are the unit vectors of the laboratory frame of reference.

Since the thermal relaxation time for water sample is about $3s$, which is of the same order of magnitude as well as the holding field sweep time $T_{sweep} = 5.83s$.

In order to find an analytic solution we first assume that $T_{1r} = T_{2r}$ and polarization follows the effective magnetic field $\vec{H_{eff}} = (H - H_\circ)\hat{z}' + H_1\hat{x}'$ provided that the adiabatic conditions are satisfied. In this case the set of Bloch equations reduces to one equation. The integral form of the solution is

$$P(t) = e^{-(t-t_\circ)/T_1}(P(t_\circ) + \frac{1}{T_1}\int_{t_\circ}^{t} e^{(t'-t_\circ)/T_1} P_{eq}(t)dt') \tag{3.28}$$

which gives an approximate analytic solution of the Bloch equations. The analytic solution allows one to fit the water signal and determine the signal height.

Since the AFP signal is proportional to the spin magnetization, one can scale the water signal to calculate the calibration constant κ_w between the ^3He signal height S_{He} and polarization P_{He} using $P_{He} = \kappa_w S_{He}$ where ω stands for water calibration [23] .

3.3 Adiabatic Fast Passage process and conditions

A. Adiabatic Fast Passage

From the equation of motion (3.8) we may immediately deduce

$$\frac{dM^2}{dt} = 2\vec{M}\frac{\vec{M}}{dt} = 0. \tag{3.29}$$

The magnitude of the magnetization M is a constant of the motion, whatever the variation of H with time. It will now be shown that if this variation is sufficiently slow, the angle of the magnetization with the instantaneous direction of the field is also a constant of the motion.

The variation with time of the vector $\vec{H}$ can be described quite generally by the vector equation

$$\frac{d\vec{H}}{dt} = \vec{\Omega} \times \vec{H} + \Omega_1 \vec{H}, \tag{3.30}$$

where the vector $\vec{\Omega}$ and the scalar Ω_1 have the dimensions of a frequency. Consider a moving frame S' where the z-axis is continuously aligned along the instantaneous direction of the field $\vec{H}$. According to the Eq. (3.30) the relative motion of S' with respect to the laboratory will be a rotation about an instantaneous axis $\vec{\Omega}$. In that frame the magnetization will change in time according to

$$\frac{\partial M}{\partial t} = \gamma \vec{M} \times (\vec{H} + \frac{\vec{\Omega}}{\gamma}). \tag{3.31}$$

By definition, in this frame $H_x = H_y = 0$ and

$$\frac{\partial M_z}{\partial t} = M_x \Omega_y - M_y \Omega_x. \tag{3.32}$$

If $|\Omega| \ll |\gamma H|$ then, approximately,

$$\frac{\partial M_x}{\partial t} \cong \gamma H M_y, \qquad \frac{\partial M_y}{\partial t} \cong -\gamma H M_x, \tag{3.33}$$

M_x and M_y are approximately sinusoidal functions with instantaneous frequency $\omega_0(t) = -\gamma H(t)$.

After a long time t, the change in M_z will be

$$\Delta M_z = M_z(t) - M_z(0) = \int_0^t [M_z(t')\Omega_y(t') - M_y(t')\Omega_x(t')]dt. \tag{3.34}$$

If the variation of Ω with time is sufficiently slow, or to be precise, if its Fourier expansion has neglible components at frequencies of the order of $|\gamma H(t)|$, then for any t,

$$|\Delta M_z| \sim |\frac{M\Omega}{\gamma H}| \ll M, \tag{3.35}$$

and M_z, that is, the component of $\vec{M}$ along the field, will remain constant. This result may be applied to the case of a magnetic moment in a rotating field $\vec{H}_0 + \vec{H}_1$ of the type previously defined where the D.C. field is being slowly varied. From the definition of the effective field H_{eff} we have

$$\frac{d\vec{H}_{eff}}{dt} = \cos\theta \frac{\dot{H}_\circ}{H_{eff}} \vec{H}_{eff} + \sin\theta \frac{\dot{H}}{H_{eff}} (\hat{n} \times \vec{H}_{eff}) \tag{3.36}$$

where $\hat{n}$ is a unit vector orthogonal to $H_\circ$ and H_1. Comparing this with equation (3.30) gives

$$\Omega = \sin\theta \frac{\dot{H}_\circ}{H_{eff}} = H_1 \frac{\dot{H}_\circ}{H_{eff}} \tag{3.37}$$

The quantity Ω is the smaller, the farther from the resonance. From the adiabatic condition $|\Omega| \ll |\gamma H_{eff}|$ we have

$$\dot{H}_\circ \ll \frac{\gamma H_{eff}^2}{\sin\theta}. \tag{3.38}$$

This condition is strongest at resonance and gives

$$\dot{H} \ll \gamma H_1^2. \tag{3.39}$$

For the applicability of the adiabatic theorem [14] we also require that the spectrum of $\Omega(t)$ contains no frequencies comparable to γH_{eff}. If the time variation of $H_\circ$ is a modulation $H_\circ = H_\circ^* + H_m \cos\rho t$ this requires $\rho \ll |\gamma H_1|$, whereas (3.39) becomes $\rho H_m \ll \gamma H_1^2$. If we superimpose the condition $H_m \gg H_1$, which is not incompatible with the previous ones, the duration $\tau = |\frac{H_1}{H_\circ}|$ of the resonance will be a small fraction of the modulation period [30].

If we start from a value of $H_\circ$ say far above resonance where the effective field is practically parallel to $H_\circ$, and go through the resonance to the other side, far below the resonance, the magnetic moment $\vec{M}$, initially parallel to $\vec{H}_\circ$, will remain continuosly parallel to $\vec{H}_{eff}$ and thus, end up antiparallel to $\vec{H}_\circ$. At the passage through the resonance there will be a transverse magnetization equal to the initial value M_{eff}. If there is a distibution of Larmor frequencies, the magnetic moment of the sample can still be reversed by adiabatic passage, since the condition (3.39) is in independent of the width δ of the shape function. However, the maximum value of the transverse magnetization during the passage is reduced in a ratio of the order of ω_1/δ if $\delta \gg |\omega_1|$.

B. Conditions of adiabatic fast passage

During polarization, the ^3He magnetic moments are anti-aligned with the strong, magnetic holding field $H_\circ\hat{z}$. For a number density N of ^3He spins with polarization P, the net magnetization is

$$\vec{M} = NP\vec{\mu} \tag{3.40}$$

Since the ^3He magnetic moment $\mu_{^3He}$ is negative, $\mu_{^3He} = -1.064 \times 10^{-26}\frac{J}{G}$, the ^3He net magnetization points in a direction opposite to that of the magnetic moments.

After polarization, a weak RF field $\vec{H}_{RF} = 2H_1\cos(\omega_1 t)\hat{x}$ is applied where $H_1 \ll$

$H_\circ$. In the frame rotating at $\vec{\omega}_1 = -\omega_1 \hat{z}$, an effective magnetic field $\vec{H}_{eff}$ is produced (Eq. (3.23). Initially $H_\circ \ll \frac{\omega_1}{\gamma}$ and is below resonance. The effective magnetic field $\vec{H}_{eff}$ is therefore aligned with the ^3He magnetization in the $-\hat{z}'$ direction.

During AFP, $\vec{H}_{eff}$ is rotated about $\hat{y}'$ at a speed slow enough for the ^3He magnetization to follow the rotation adiabatically. Since $\hat{z}' = \hat{z}$, an $\vec{H}_{eff}$ rotation from $-\hat{z}'$ to $\hat{z}'$ in the rotating frame will correspond to a reversal in the direction of ^3He magnetization and polarization in the laboratory frame. The rotation of $\vec{H}_{eff}$ is achieved by ramping $H_\circ$ at constant speed $\frac{dH_\circ}{dt}$ from below resonance ($H_\circ \ll \frac{\omega_1}{\gamma}$) to above resonance ($\frac{\omega_1}{\gamma} \ll H_\circ$). Typically, the field is then ramped back down to below resonance to restore the initial direction of polarization.

For the spins to follow $\vec{H}_{eff}$ adiabatically, they must precess about $\vec{H}_{eff}$ much faster than $\vec{H}_{eff}$ rotates about $\hat{y}$ [29]. Since $\frac{dH_\circ}{dt}$ and H_1 are constant, the maximum rate of $\vec{H}_{eff}$ rotation $\frac{d\theta}{dt}$ about $\hat{y}'$ occurs at resonance where

$$\frac{d\theta}{dt} = \frac{1}{H_{eff}} \frac{dH_\circ}{dt} \tag{3.41}$$

and

$$H_{eff} = H_1 \tag{3.42}$$

At resonance the spins precess at ω_1. This sets the adiabatic condition as

$$\frac{1}{H_1} \frac{dH_\circ}{dt} \ll \omega_1 \quad (= \gamma H_1) \tag{3.43}$$

Relaxation mechanisms dominate during passage through resonance. Longitudinal and transverse relaxations (with respect to $\vec{H}_{eff}$) are described by two time constants, T_{1r} and T_{2r} respectively. In the rotating frame, the magnetization is always aligned with $\vec{H}_{eff}$, and therefore T_{1r} dominates. The time spent near resonance

must be short with respect to T_{1r} to maintain polarization and achieve a polarization signal. At resonance $|\vec{H}_{eff}|$ is at a minimum, and consequently T_{1r} is shortest. The fast condition

$$\frac{1}{T_{1r}} \ll \frac{1}{H_1}\frac{dH_\circ}{dt} \tag{3.44}$$

is therefore placed upon the ramping speed $\frac{dH_\circ}{dt}$ at resonance ($H_{eff} = H_1$). Combining Eq. (3.43) and Eq. (3.44) gives the complete condition for adiabatic fast passage

$$\frac{1}{T_{1r}} \ll \frac{1}{H_1}\frac{dH_0}{dt} \ll \gamma H_1 \tag{3.45}$$

In NMR systems similar to this one, T_{1r} is dependent on the ^3He diffusion constant and magnetic field inhomogeneities [27]. By comparison, it is expected that T_{1r} is on the order of 500 seconds. At typical experimental parameters ($H_1 = 80$ mG, $\frac{dH_\circ}{dt} = 1.2$ $\frac{G}{s}$) the conditions for adiabatic fast passage are well satisfied:

$$(\frac{1}{T_{1r}} = 0.002s^{-1}) \ll (\frac{1}{H_1}\frac{dH_\circ}{dt} = 15s^{-1}) << (\gamma H_1 = 1630s^{-1}) \tag{3.46}$$

At resonance ($H_\circ = \frac{\omega_1}{\gamma}$), $\vec{H}_{eff}$ and the ^3He net magnetization are in the $\hat{x}'$ direction. In the laboratory frame, this is seen as the net magnetization rotating about $\hat{z}$ at the angular frequency ω_1. The magnetizations frequency of rotation ω_1 is equivalent to the oscillation frequency of the RF field. The rotating magnetization $\vec{M}_R$ creates an oscillating magnetic flux within two parallel coils of wire (the pickup coils) near the ^3He. An emf $\xi \propto \vec{M}_R \propto P$ oscillating at ω_1 is induced in the pickup coils. Using various electronics described in the next section, this voltage (polarization signal) is measured and recorded.

Chapter 4

Calibration of Equipment

The setup for polarization measurements uses a variety of electronics, and set of magnets. In this chapter experimental setup and experimental procedures are described. Instrument synchronization is also noted.

4.1 Experimental Setup

Our experimental setup consists of several coils set shown in the Figures 4.1, 4.2 and mounting rack with electronics as can be seen from Figures 4.3, 4.4.

A. Set of Coils

1. Hemlholtz coils

   Efficient polarization and accurate adiabatic fast passage measurements require a very homogeneous holding magnetic field. This homogeneity is provided by a pair of Helmholtz coils shown in the Fig. 4.1. These coils were manufactured by Walker Scientific LDJ, Inc. Helmholtz coils (main coils) with overall outer diameter 55.0 inches, central field at rated operating current 36.0 G, nominal

inductance 140 mH and resistance (per coil pair at 70 F) 2.15 Ω. Specification of Helmholtz coils system is given in the Table 4.1.

Fig 4.1: Helmholtz coil system.

Table 4.1: Specification of Helmholtz coil system

Specification	Helmholtz	RF coils
Area of Uniformity	$40 \times 4 \times 15\ cm^3$	
Uniformity	1 %	
Overall I.D.	49.5 in.	31 in.
Overall O.D.	55 in.	33.75 in.
Nominal Intercoil Spacing (face to face)	24 in.	15.75 in.
Resistance (per coil pair at 70^oF)	2.15	.75
Rated Operating Current	14.4 Amps	2 Amps
Central Field at Rated Operating Current	36 Oe	.175 Oe
AC Operation	NO	YES
Nominal Inductance	140 mH	.111 mH

2. RF coils

   The smaller set of coils, the RF coils, are fixed perpendicular to the main coils and provide the RF field (91 kHz, 80 mG peak-to-peak) used in AFP experiments. The RF coils have 0.7 Ω resistance, 0.114 mH inductance, 15.00 inches separation (face to face), 33.75 inches outer diameter, and 31.0 inches inner diameter.

3. Pick-up coils

   The role of the third pair of coils shown in the figure 4.2, pick-up coils is to detect the signal from polarized sample. These coils located at the geometrical center of Helmholtz coil system allow precise alignment orthogonal to the RF coils. If the pick-up coils are not exactly aligned orthogonally to the RF field, signals from the RF coils (seen as noise) will prevent measurement of the

polarization signal. Each pick-up coil comprises 150 turns of Belden 8084 36AWG Heavy Polythermaleze wire wrapped in a 0.16 inches groove around a rectangular area 0.75 inches by 4.33 inches of PVC plastic. Each coil has a 36 Ω resistance, a 1.4 mH inductance, and is connected to the A and B channels of a Preamplifier.

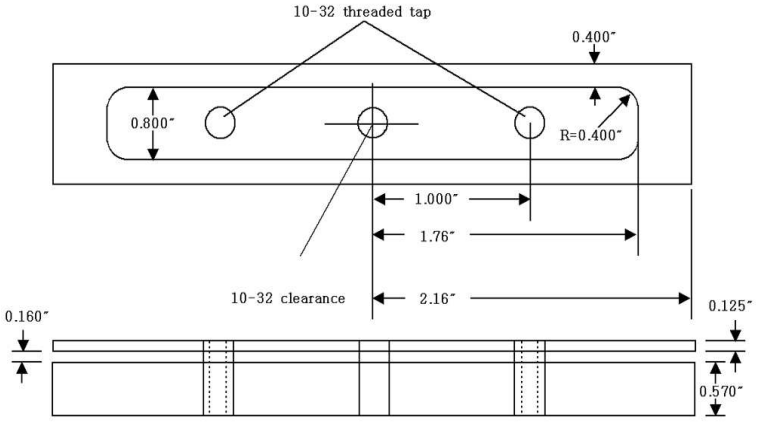

Fig 4.2: Schematic design of pick-up coils.

B. Electronics

This section of the thesis describes electronics setup. NMR setup schematic is shown in the Figure 4.3. Text below is referred to that figure.

1. Kepco Power Supply

   Power supply's output effect must be less than $10^{-4}\%$ of maximum rated voltage, A KEPCO Bipolar Operational Power Supply (BOP) satisfies this requirement with mentioned parameter value $5 \times 10^{-5}\%$. It powers the main coils in series, output voltage varies with time from 21 to 29 Volts. The BOP has two bipolar control channels (voltage or current mode), selectable and individually

controllable either from front panel controls, or by remote signals. The BOP initially is used in Voltage Mode, where no preventing noise has been observed as recommended by Sebastien Inserti, TJNAF [31].

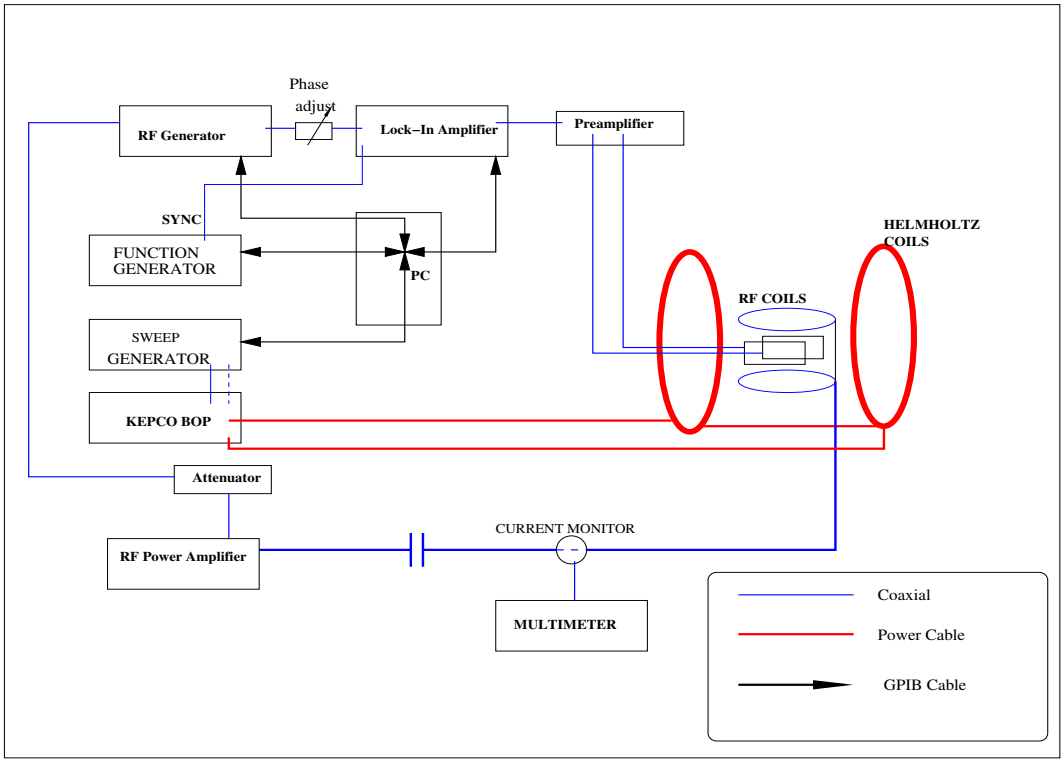

Fig 4.3: Schematic of NMR Setup.

The BOP output can be programmed over its full output range by a $\pm 10V$ signal applied to either one of the inputs to the voltage or the current channel. For that reason, BOP is connected to a function generator.

2. Function Generator

The Synthesized Function Generator, Stanford Research Systems DS345 can sweep the output frequency of a function over wide range of allowable output

frequencies without restrictions on minimum or maximum sweep span. Function generator controls Kepco BOP Supply to sweep holding magnetic field with time for an AFP experiment. A DC voltage V_{FG} on the function generator sets a corresponding DC voltage $V_{Kepco} = 3.59V_{FG} + 0.012V_{rms}$ at the Kepco power supply outputs.

3. RF Generator

   The RF excitation of the power amplifier is produced by RF generator, Agilent Technologies Model 32250 A. It delivers a sine wave at 91 kHz with an amplitude of 2.4 V_{rms} and zero offset level to the power amplifier via the Very High Frequency attenuator.

4. VHF Attenuator

   Input Very High Frequency (VHF) Attenuator, Agilent Technologies 355D (30 dB) is used to limit and therefore protect the amplifier from excessive amplification. An input voltage of 2.4 V from the RF function generator corresponds to about 3.3 A peak-to-peak through the RF coils.

5. Current Monitor

   The Current Monitor, toroid built by Pearson Company, intersected by one of the RF drive line wires going to the RF coils. The induced voltage monitored online by a multimeter in order to measure the current through the RF coils. The current monitor is calibrated such that a 1 V_{rms} output indicates 1 A_{rms} is passing through the wire.

6. RF Lock-in Amplifier

   Lock-in amplifier, Stanford Research Systems Model SR844, used in this study has a single-ended BNC Voltage input, 50 Ω impedance, and $25kHz$ to $200MHz$

bandwidth; This lock-in amplifier uses a technique known as phase sensitive detection to single out the component of the signal at a specific reference frequency and phase. Noise signals at frequencies other than the reference frequency are rejected and do not affect the measurement. The lock-in amplifier is connected to the output of the preamplifier which amplifies induced voltage in the pick-up coils. Lock-In amplifier extracts the Fourier component of the signal at 91 kHz, as referenced with synchronized signal (square shape wave) of the RF excitation function generator. The induced voltage appears in two display channels (X and Y), one of which contains only the actual induced voltage and the other contains only noise. The phase of the lock-in amplifier can be set manually in order to reject all the noise in one of those two channels.

7. Preamplifier

   The low noise preamplifier, Stanford Research Systems SR560, output is the differential of two channels (A - B) incoming from pick-up coils. This preamplifier uses a $6dB$, $10kHz$ high-pass filter and $6dB$ $100kHz$ low-pass filter to aid in isolating the 91 kHz signal. The preamplifier also has incremental gain settings that are used during coil alignment. It is sensitive to external noise sources. Priority must be given to use in battery power mode, where the noise level is less than from AC line power mode.

8. RF power amplifier

   The linear amplifier, $AT\&C$ Power Conversion ULTRA 2021 $100Watt$, will be dedicated as RF power amplifier. The RF power is amplified by RF power amplifier before being sent to the RF coils. It receives the excitation from a dedicated function generator and sends it toward the RF coils. A capacitor is used in this circuit to reduce reflected power into the RF amplifier. Reflected

power (due to the reactive nature of the load) is potentially damaging to the amplifier in addition to causing heating and instability within the unit. A $50nF$ capacitor counterbalances the inductive impedance of the RF coils.

Fig 4.4: Mounting Rack with Electronics.

9. Gaussmeter, Multimeters and Oscilloscope

   The Gaussmeter, Lake Shore Cryotronics, Inc Model 450 with axial and transverse Hall Generators (Gaussmeter Probes) is used to monitor magnetic field of main coils. Multimeter, Fluke 45 is connected to BNC output of the current

monitor to display induced voltage. Another multimiter of the same make is used for measure output voltages of the devices. We used Digital Oscilloscope, Tektronix Model TDS-2012.

10. GPIB interface

    The lock-in amplifier, function generator and RF generators are GPIB interfaced for computer control and data recovery.

4.2 Experimental Procedures

A. General Method of Polarization Measurements

The sample in cell is placed in an homogenous magnetic field produced by a Helmholtz coil pair. At the same time an RF field is produced by a second pair of coils orthogonal to them. The AFP sweep is produced by holding the RF frequency fixed and sweeping the main magnetic field through the RF resonance. At resonance, the spins flip and this is detected by a pair of pick-up coils wrapped around the cell. Quality factor $Q \propto L/r$ of the coil 100 is reasonable order [14]. The induced AC voltage in the pickup coils is detected with a lock-in amplifier referenced to the RF frequency. Usually absolute polarization can be determined by calibrating the NMR apparatus with a water sample. The polarization of the water sample is known in advance, as it follows a Boltzman distribution for thermal equilibrium situation. From the Faraday law one could calculate the voltage at the terminals of the coil. The susceptibility of the protons 3×10^{-10} in water at room temperature. Finally this calculation depends how sample fills inside of the coil entirely (filling factor). The voltage proportional to its parallel impedance is proportional to filling factor. Quality factor and complex RF susceptibility, which can be expressed by suggesting that the inductance of the pickup coils, in the presence of nuclear magnetization takes the complex value.

The nuclear signal appears as a very small modulation on the voltage that exits in its absence. The AFP is the only method that give tolerable signal-to-noise ratios (SNR) [14].

B. Evaluation of Flux Density of Radio Frequency field using Detection Loop

The RF field generation system is described in section 4.1 of this thesis. The principle of the measurement is the following: RF field is applied to the detection loop connected to multimeter input, inducing voltage in its wires thereby might be measured online.

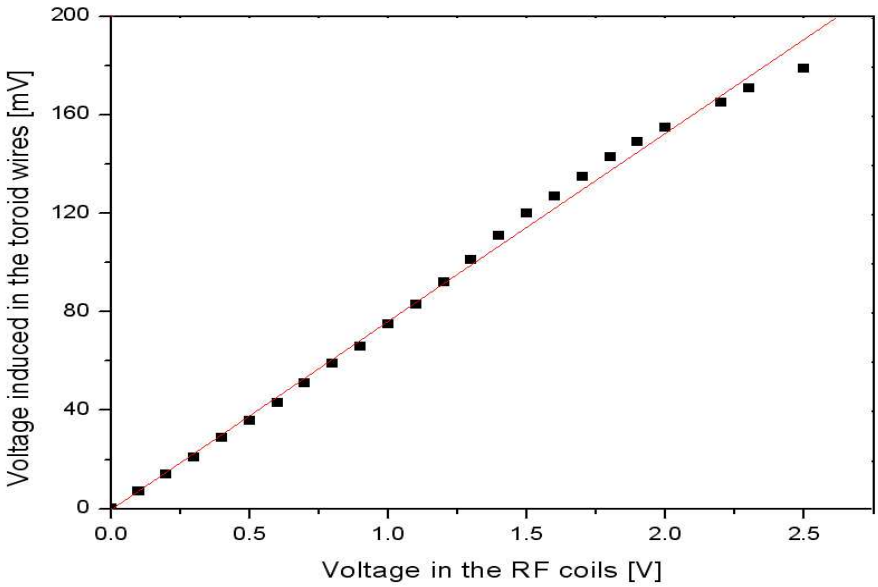

Fig 4.5: Variation of induced voltage with RF signal amplitude adjustment, comparison with theoretically predicted straight line.

Toroid was constructed from nonmagetic material, diameter $D = 3 \times 10^{-2}\ m$ and $n = 30$ number of turns of AGW 28 wire. RF generator settings were: sine form

signal with frequency 91 kHz, amplitude 2.0 V, offset 0.0 V.

The first experiment was performed with constanti RF voltage of 2.0 V. The detection loop placed horizontally at the geometrical center of the RF coils. Attenuation was swept from 153 dB to 226 dB.

In the second experiment position of detection loop remained the same as in the first experiment. Measurements were done at attenuation level of 25 dB at 91 kHz. The RF voltage magnitude, V_{rms} was swept in step of 0.1 V in order to see the response of other apparatus. Another multimeter detected voltage induced on Pearson Current Monitor i.e. voltage in the wires of RF coils. Figure 4.5 shows variation of voltage induced in the toroid wires with voltage in the RF coils change. Induced voltage V in the detection loop was obtained from the Lenz law:

$$V = \frac{d\phi}{dt} = \omega\phi \tag{4.1}$$

where ϕ is the flux of magnetic field component of the RF field H_1; the circuit is running at a pulsation $\omega = 2\pi f$, f is the frequency of RF field.

The RF field H_1 is obtained from:

$$\begin{aligned} B = 2H_1 &= \frac{V_{PeaktoPeak}}{4\pi f S} \\ &= 6.3 \times 10^{-5}\, Tesla = 0.63\, Gauss \end{aligned} \tag{4.2}$$

where $V_{PeaktoPeak}$ is an amplitude of RF field, it is equal to V_{rms} because offset level is zero. S is the loop section:

$$S = \frac{n\pi D^2}{4} = 0.021\ m^2$$

Note: RF field amplitude $V_{PeaktoPeak} = V_{rms} = 1.6\,V$, RF power amplifier Forward Power 16 $Watt$, Attenuation 25 dB are default settings when performing the NMR measurement for ^3He.

C. Q-curve measurement

The Q-factor of the pickup coil circuit is needed to adjust polarization data from experiments. Q-curve, variation of induced voltage in the pickup coils with frequency was measured (Fig. 4.6). To measure Q-curve, Q-Loop was constructed with 100 turns of wire and aligned parallel to the pick-up coils. For experimental purposes RF power amplifier and RF coils are disconnected from schematic shown in Figure 4.3. Instead Q-Loop was connected to be directly powered by RF function generator. This loop is used to create an oscillating field that is detectable by the pick-up coils.

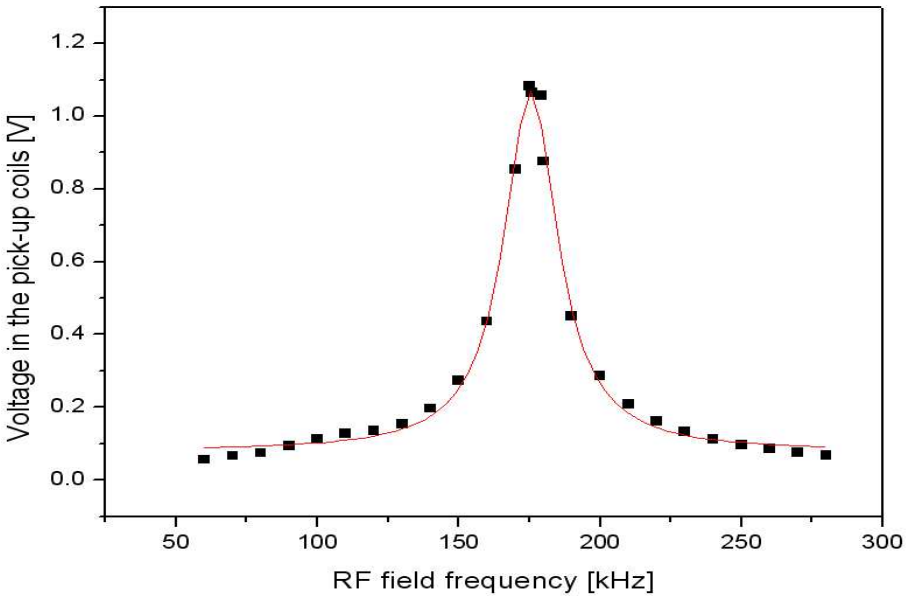

Fig 4.6: Experimentally obtained Q-curve fitted with Lorentzian. The resonance (175 kHz) was designed to be away from 91 kHz for stability.

Pick-up coils voltage Modulus and Phase from preamplifier were monitored using lock-in amplifier. Preamplifier has DC filter cutoffs and coupling, low noise gain set to 20, A-B source mode, $V_{rms} = 200mV$ and zero offset level. Frequency of RF generator was swept from 50 kHz to 300 kHz, in steps of 1 kHz.

D. NMR system response to external source signals

Investigation of the setup response to signals arising from external sources has significant importance for further experiments. Several careful experiments were modeled for the NMR Setup with specially designed loop, diameter 1", 50 turns of AGW 28 wire. The loop was attached to the output of RF function generator, DS345. It radiates signal which is received by the NMR receiver through the pick-up coils. Preamplifier in A-B mode supplies amplified signal to the lock-in amplifier. Data from both outputs of the lock-in amplifier were digitized and recorded by computer. The phase was adjusted to maximize the signal in one of the lock-in amplifier display channels. Lock-in amplifier makes average of data obtained during 50 runs in its buffer and sends it to computer.

Experiments proceed in the following manner:

1. Connect a loop to the output of the RF function generator instead of RF power amplifier and RF coils.
2. Turn NMR Setup and computer power buttons on.
3. Set Kepco BOP to Voltage mode, minimal voltage 25 V, maximal 32 V.
4. Turn Kepco BOP A-C circuit breaker/power switch to ON position.
5. Fix loop at desired distance from pick-up coils.
6. Set synchronizing function generator and RF function generator settings.

7. Run the programs "NMR Load Sweep.vi" and "NMR XY reading.vi" to start holding magnetic field sweep and reading data from lock-in amplifier respectively.

8. Prevent overload on preamplifier and lock-in amplifier if necessary by choosing appropriate gain values.

9. Use knob to adjust phase to maximize lock-in amplifier channel X displayed values.

10. Wait for plots.

11. Repeat the steps 9, 10 again because with the time passes phase adjustment may be necessary.

12. Go to step 5.

13. Stop the experiment by closing mentioned programs. Turn off computer and then power of the rack with electronics.

E. Observation of signal from DPPH

Usually absolute polarization is determined by calibrating the NMR apparatus with a deionized water sample. The polarization of water sample is known in advance, as it follows from Boltzman distribution for thermal equilibrium situation. The susceptibility of protons in water is 3×10^{-10} at room temperature. The nuclear signal appears as a very small modulation on the voltage that exists in signal's absence. The most troublesome factor in performing a water calibration is the poor Signal to Noise Ratio (SNR). That is why a stable free radical 2,2-Diphenyl-1-Picrylhydrasyl (DPPH) with g-factor $g = 2.039 \pm 0.023$ is an alternative material for a calibration measurements [20].

One can show the thermal equilibrium polarization for DPPH:

$$P_{DPPH} = \tanh(\frac{m_B}{kT}) \tag{4.3}$$

where k is a Boltzman constant, T temperature of the sample and m_B is a Bohr magneton for electron, which is about 2000 times larger than proton magneton.

SNR could be good enough depending on the quantity of the material, 3 cm^3 of DPPH is satisfactory [19]. For polarization measurements of ^3He cell we should use relation of measuring signals for ^3He and DPPH. Method of calculation could be same as it is for water calibration is obtained from ratio:

$$\frac{Gain_{^3He} \times \mu_{^3He} \times \rho_{^3He} \times signal_{^3He}}{Gain_{DPPH} \times \mu_{DPPH} \times \rho_{DPPH} \times signal_{DPPH}} \tag{4.4}$$

where $Gain_{^3He}$ ($Gain_{DPPH}$) is a gain value of preamplifier during ^3He (DPPH) polarization measurements experiments run, $\mu_{^3He}$ (μ_{DPPH}) is a dipole magnetic moment of ^3He nuclei (DPPH electrons), $\rho_{^3He}$ (ρ_{DPPH}) is the density of ^3He gas (DPPH powder) at experiments run, and $signal_{^3He}$ ($signal_{DPPH}$) is ^3He (DPPH) signal voltage magnitudes.

The DPPH sample, 5 grams in an ampoule wrapped with two pick-up coils (10 turns of AGW 28 wire each) is placed at the geometrical center of the Helmholtz coil system. Experiment is performed on NMR Setup (Figure 4.3), and explained in details in section 4.1 of this thesis.

In order to satisfy AFP conditions the magnitude of the RF field, frequency, and holding magnetic field sweep rate are adjusted: RF generator voltage amplitude and frequency are set 2.30 V_{rms} and 91 kHz respectively. The holding magnetic field is swept from 0 to 7 $Gauss$ with the rate of 1.2 $Gauss/sec$. The lock-in amplifier phase angle is $-148.17°$. VHF attenuator kept at 30 dB. Preamplifier powered by AC line has the following settings: amplification gain of 200, DC coupling, low noise

option, offset level equal to zero, output A-B configuration and bandpass filter set to 10 kHz to 100 kHz. Holding magnetic field sweep, synchronization and monitoring of some devices are performed using LabView programs on computer.

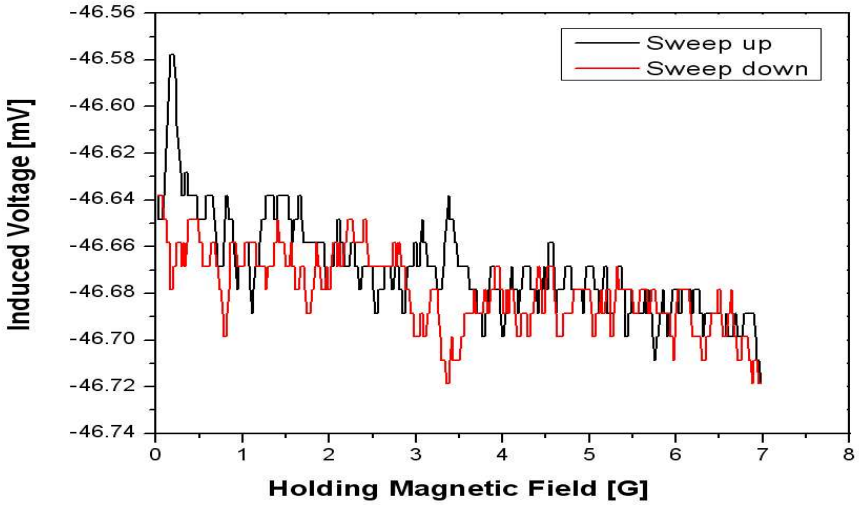

Fig 4.7: Signal from DPPH sample.

It is the best not to completely reduce the value of A-B in Y channel of lock-in amplifier using this method. It seems that either the preamplifier or lock-in amplifier enters into an unstable mode of operation when there is no residual signal from the pickup coils. The noise level increases dramatically and the NMR signal is lost to the background.

DPPH signal is shown in the Figure 4.7. The reason it has a ramp is that holding magnetic field is swept with time up and down. Background noise incoming from equipment used in neighboring laboratories could not be decreased

Chapter 5

Results and Discussion

5.1 Results

The linear relation between the magnetic field magnitude B and the voltage V in the main coils is determined by the following relation:

$$B = \alpha V + \beta \tag{5.1}$$

using a Gaussmeter. Transverse and axial Hall generators are placed at the geometrical center of the system. The power supply displays adjustments of voltage. Constant values in relation are found to be $\alpha = -3.94 \pm 0.01\ G/V$ and $\beta = -0.29 \pm 0.01\ G$.

Figure 5.1 to 5.5 show the results of experiments described in subsection C of section 4.2 focused on NMR system response to external source signals. The main goal of these experiments are to test sensitivity of lock-in amplifier to the adjustment of output characteristics of external function generator.

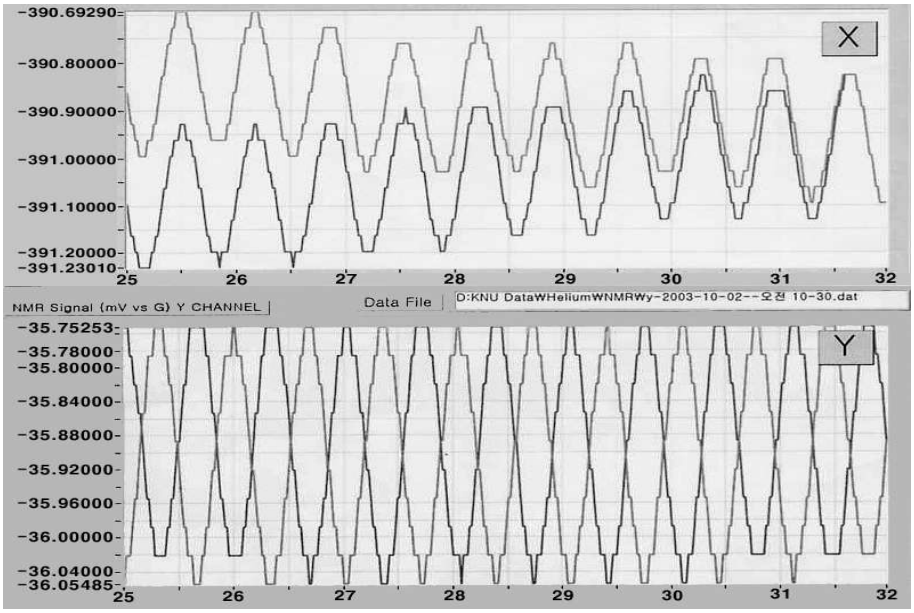

Fig 5.1: Signal shape when lock-in amplifier worked as a frequency detector.

As indicated in Figure 5.1, lock-in amplifier is working as a frequency detector: NMR receiver resonant frequency and radiation generator's frequency are 91000 Hz and 91002 Hz respectively. Distance between loop and receiver is 1 meter. Amplitude Modulation is with rate equal to 1200 Hz, modulation depth is 70%. One may judge from this figure that indeed lock-in amplifier is working properly and its response is as expected.

Channels X and Y correspondingly display absorption and dispersion by the spin system of RF power supplied by an external function generator. Each channel shows two curves which stand for two sweeps of holding magnetic field, so called "ramping up" and "ramping down".

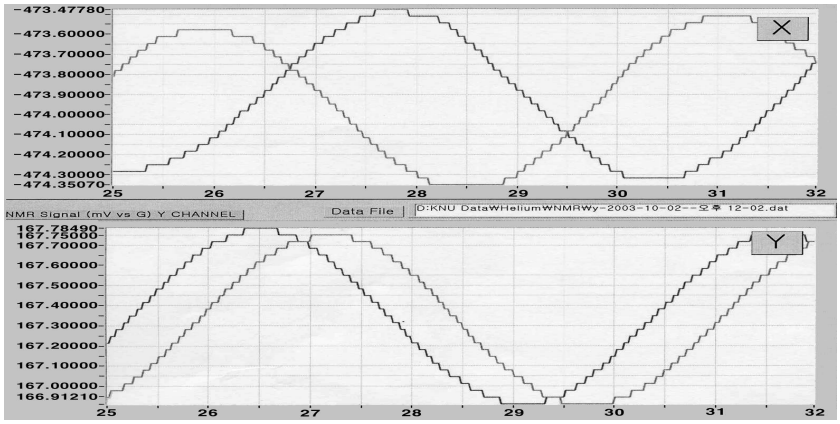

Fig 5.2: Signal detected from loop, lock-in amplifier phase set to 64.6°.

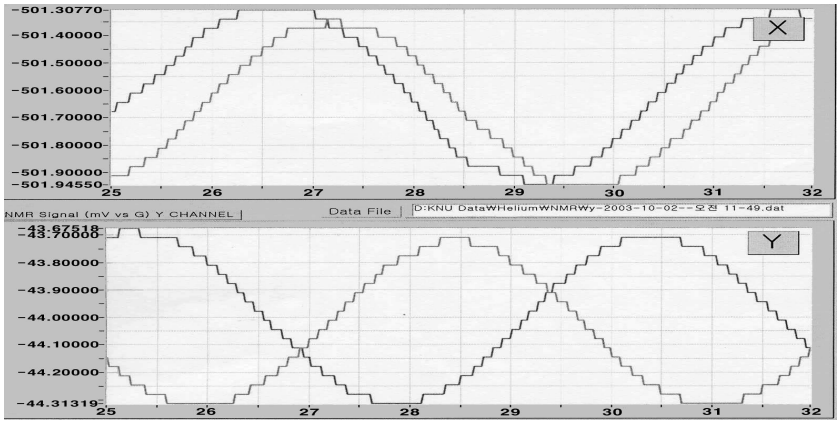

Fig 5.3: Signal detected from loop, lock-in amplifier phase set to 40.0°.

In Figure 5.2 and Figure 5.3, lock-in amplifier set as a phase sensitive detector (PSD) with distance between loop and receiver 1 meter. Phase of lock-in amplifier, 64.6° and 40.0° respectively. One may conclude that lock-in amplifier "feels" an adjustment of phase. Good phase sensitivity has significant importance for polarization measurements of wide range of polarized samples.

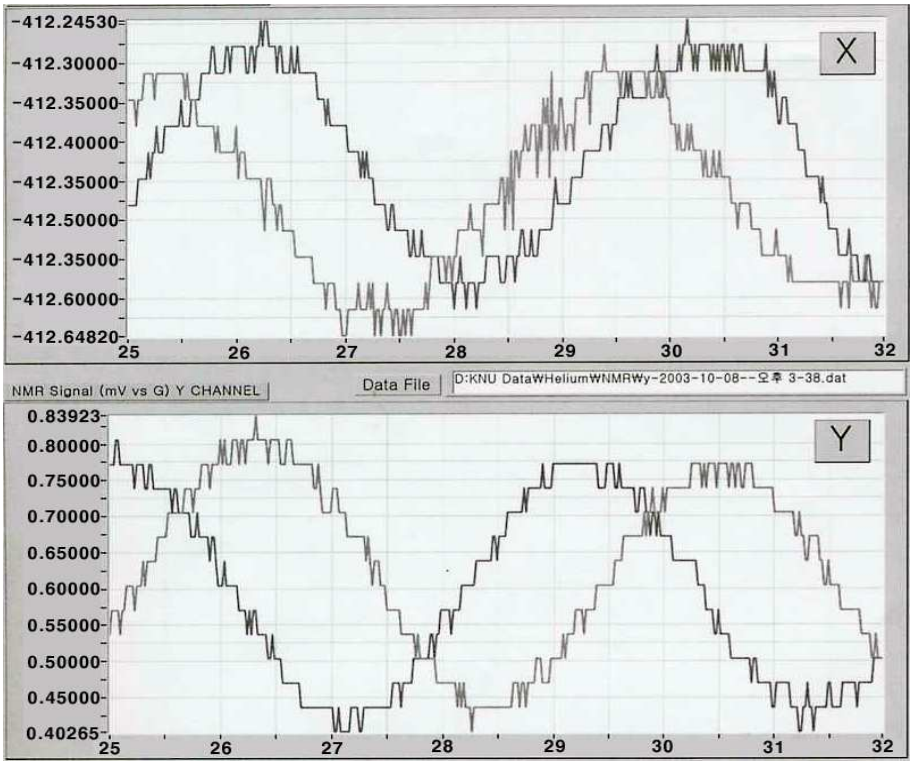

Fig 5.4: Variation of induced voltage in the pick-up coils as a function of holding magnetic field.

In the Figure 5.4 the resonance frequencies of the NMR setup and external function generator coincide, 91 kHz, modulating frequency 0.1 Hz with depth of 10%. The distance from loop to receiver distance is 3 meters. With the increase of distance the quality of the signal becomes worse. As can be seen Figure 5.4 resembles Figures 5.2 and 5.3 with the difference of "zig-zags" (noise) sitting in the sinusoidal wave.

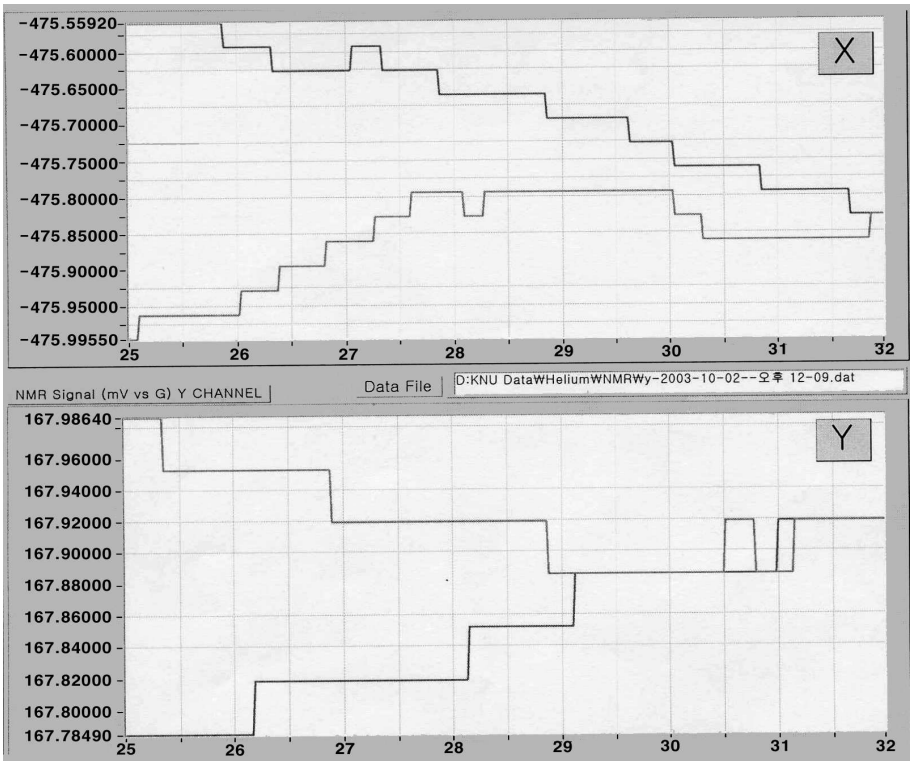

Fig 5.5: Results of measurement with RF radiation generator turned off.

Measurement of background noise level is held with RF generator off as in Figure 5.5. The reason signal has non-linear form is that holding magnetic field changes with time causing change of RF field around experimental setup and there is a noise incoming from other devices in the laboratory room.

5.2 Discussion

We have presented one possibility of ^3He polarimetry on the base of measuring the DPPH signal as a standard for calibration, which with existing methods of water calibration and frequency shift of the *Rb* Zeeman resonance could be used for

precision polarimetry of ^3He Polarized target. This could give possibility for easy operating polarization measurements.

Electronics part of NMR Setup for polarization measurement of ^3He target was successfully constructed and calibrated. It has wide application area; mainly at the measurement of neutron spin structure and high efficient Magnetic Resonance Imaging in medicine. Q-curve, variation of induced voltage in the pickup coils with frequency was measured. Remarked work to increase Signal Noise Ratio is carried. Instability modes of electronics were set to minimum or avoided. Background noise incoming from neighboring laboratories is still high. Main contributors are personal computers and vibration "microphonic" effect. The protons in the hydrogen atoms of water achieve a thermal equilibrium polarization that is calculable and is measurable using AFP. The polarization signal, however, is many orders of magnitude smaller than the expected ^3He signal, therefore is difficult to detect. The source of background noise should be searched and efforts should be made to reduce this noise in the future.

Bibliography

[1] J. D. Bjorken, Phys. Rev. D **1**, 1376 (1980).

[2] S. D. Drell and A. C. Hearn, Phys. Rev. Lett. **16**, 908 (1966); S. B. Gerasimov, Sov. J. Nucl. Phys. **2**, 430 (1966).

[3] B. G. Yerozolimsky, Nucl. Inst. and Meth. A **440**, 491 (2000).

[4] J. R. Johnson et al., Nucl. Inst. and Meth. A **356**, 148 (1995).

[5] R. M. Woloshyn, Nucl. Phys. A **496**, 749 (1989).

[6] G. Cates and Z.-E. Meziani, Thomas Jefferson National Accelerator Facility Proposal E94-101, http://hallaweb.jlab.org/physics/experiments/he3/

[7] H. Gao, Thomas Jefferson National Accelerator Facility Proposal E95-001, http://hallaweb.jlab.org/physics/experiments/he3/

[8] Z. -E. Meziani, Thomas Jefferson National Accelerator Facility Proposal E99-117, http://hallaweb.jlab.org/physics/experiments/he3/

[9] T. Averett and W. Korsch, Thomas Jefferson National Accelerator Facility Proposal E97-103, http://hallaweb.jlab.org/physics/experiments/he3/

[10] P. L. Anthony et al., Phys. Rev. Lett. **71**, 959 (1993).

[11] G. L. Greene, A. K. Thompson and M. S. Dewey, Nucl. Instr. and Meth. A **356**, 177 (1995).

[12] H. Middleton, Magn. Reson. Med. **33**, 271 (1995).

[13] M. V. Romalis et al., Nucl. Instr. and Meth. A **402**, 260 (1998).

[14] A.A. Abragam, Principles of Nuclear Magnetism, Oxford University Press (1999).

[15] M. V. Romalis, Laser Polarized ^3He target used for a precision measurement of the neutron spin structure, Ph.D. thesis, Princeton University (1997).

[16] K. Slifer, Improving SNR for water calibration of the polarized ^3He NMR system, Polarized ^3He Lab. Technical Notes, Temple University (2001).

[17] D. E. Milkie, Polarization and Polarimetry of ^3He, B.S. thesis, College of William and Mary (2002).

[18] J. L. Knowles, Investigation of techniques for Producing High Polarization ^3He Gas Targets, B.S. thesis, College of William and Mary (2002).

[19] J. H. Lee and D. B. Min, Nuclear magnetic resonance (NMR) study on the electron donating ability of β-carotene by using 2,2-dyphenil picrylhydrazyl (DPPH), 2002 Annual Meeting and Food Expo - Anaheim, California.

[20] T. E. Chupp, R. J. Hoare, R. L. Walsworth and Bo Wu, Phys. Rev. B **72**, 2363 (1994).

[21] R. K. Harris, Nuclear Magnetic Resonance Spectroscopy, Pitman (1983).

[22] J. H. Nelson, Nuclear Magnetic Resonance Spectroscopy, Prentince Hall (2003).

[23] K. Kramer, A Search for Higher Twist Effects in Neutron Spin Structure Function $g_2^n(x, Q^2)$, Ph.D. thesis, College of William and Mary (2003).

[24] B. Larson, O. Hausser, P. P. J. Delheij, D. M. Whittal and D. Theissen, Phys. Rev. C **44**, 3108 (1991).

[25] N. R. Newbury, A. S. Barton, G. D. Gates, W. Happer and H. Middleton, Phys. Rev. A. **48**, 4411 (1993).

[26] G. D. Cates, S. R. Schaefer and W. Happer, Phys. Rev. A **37**, 2877 (1988).

[27] G. D. Cates, D. J. White, T. R. Chien, S. R. Schaefer and W. Happer, Phys. Rev. A **38**, 5092 (1988).

[28] J. E. Mellor, Investigation of a Sol-Gel Coating Technique for a Polarized ^3He Target Cells, B.S. thesis, College of William and Mary (2001).

[29] J. G. Powles, Proc. Phys. Soc. **71**, 497 (1958).

[30] F. Bloch, A. Siegert, Phys. Rev. **57**, 522 (1940).

[31] Thomas Jefferson National Accelerator Facility E94-010 Experiment Technical Notes

[32] S. Meiboom, Z. Luz and D. Gill, J. Chem. Phys. **44**, 546 (1996).

[33] R. E. Glick and K. C. Tewari, J. Chem. Phys. **44**, 546 (1996).